# Formal Bayesian Approach to GRAPPA Image Reconstruction

Chase J. Sakitis [a], Daniel B. Rowe [a]

[a] *Department of Mathematical and Statistical Sciences, Marquette University, Milwaukee Wisconsin, USA*

## Abstract

In fMRI, capturing brain activation during a physical task is dependent on how quickly volume *k*-space arrays are obtained. Acquiring full *k*-space arrays, which are reconstructed into images using the inverse Fourier transform (IFT), that make up volume images can take a considerable amount of scan time. Under-sampling *k*-space reduces the scan time, but results in aliased, or "folded," images. GeneRalized Autocalibrating Partial Parallel Acquisition (GRAPPA) is a parallel imaging technique that yields full images from subsampled arrays of *k*-space. GRAPPA uses localized weights, which are estimated pre-scan and fixed over time, to fill in the missing spatial frequencies of the subsampled *k*-space. Here, we propose a Bayesian approach to GRAPPA (BGRAPPA) where prior distributions for the unacquired spatial frequencies, localized weights, and *k*-space measurement uncertainty are assessed from the *a priori* calibration *k*-space arrays. The prior information is utilized to estimate the missing spatial frequency values from the posterior and reconstruct into full field-of-view images. Our BGRAPPA technique successfully reconstructed a simulated, single slice image with no aliasing artifacts and stronger power of task detection.

**Key Words:** Bayesian, GRAPPA, fMRI, reconstruction

## 1. Introduction

### 1.1 Background

Magnetic resonance imaging (MRI) is a type of medical imaging that creates images using magnetic fields. Functional (fMRI) was developed in the early 1990's as a technique to noninvasively observe the human brain in action without exogenous contrast agents (Bandettini et al., 1993). This procedure examines brain activity by detecting changes in the blood oxygenation using the blood-oxygen-level dependent (BOLD) contrast (Ogawa et al., 1990). When a neuron fires, the BOLD contrast increases in the proximity of the neuron and is thus a correlate for neuronal firing. Measurements are arrays of complex-valued spatial frequencies called *k*-space (Kumar, Welti, and Ernst, 1975). These *k*-space arrays are then reconstructed into images using an inverse Fourier transform (IFT). The real and imaginary part of an IFT matrix is pre-multiplied with the real and imaginary part of the *k*-space array respectively. Then the transpose of the IFT is used to post multiply *k*-space with the respective real and imaginary parts to reconstruct the real and imaginary components of the brain image (Rowe, 2016). In fMRI, the magnitude and phase of the complex-valued reconstructed images are generally utilized for analysis (Rowe and Logan, 2004; Rowe, 2005). In fMRI, measuring full arrays of data for all the slices that form the volume image typically takes about one to two seconds, limiting the temporal resolution of the obtained images and potentially diminishing brain activity detection. With hundreds of volume images commonly used for a full fMRI time series, this acquisition time of full volume k-space arrays causes the overall scan time of the experiment to be considerable. A great deal of work has been dedicated to reducing the acquisition time of the in the MRI process by accelerating the number of images obtained per unit of time. Hyde et al. (1986), Pruessmann et al. (1999), and Griswold et al. (2002) all explore parallel imaging techniques to reduce the scan time in MRI.

### 1.2 Previous Approach

Historically, a single channel coil receiver has been utilized in fMRI to measure full-sampled *k*-space data arrays. Reducing acquisition time is the primary goal of parallel imaging. More

recently, the technology development focus has been to reduce acquisition time by measuring less data without losing the ability to form a full image. This can be accomplished by skipping lines in the *k*-space array, i.e. subsampling. To accomplish this, multiple receiver coils are utilized in parallel to obtain spatial frequency arrays which are reconstructed into coil-specific brain images.

Skipping lines in *k*-space introduces what is called an acceleration factor. The acceleration factor indicates which lines of *k*-space data are measured. For example, with an acceleration factor of $n_A = 2$, every other line horizontally in *k*-space is measured. Figure 1 shows the sequential pattern for a fully sampled *k*-space array (top left) compared to a subsampled k-space array with an acceleration factor of $n_A = 2$ (top right). This acceleration factor will cause the reconstructed coil images to appear as if the image was folded over itself, because the Fourier transform cannot uniquely map the down sampled signals. We can see an example of this in the bottom left of Figure 1 where the IFT of the subsampled *k*-space causes the brain image to be aliased.

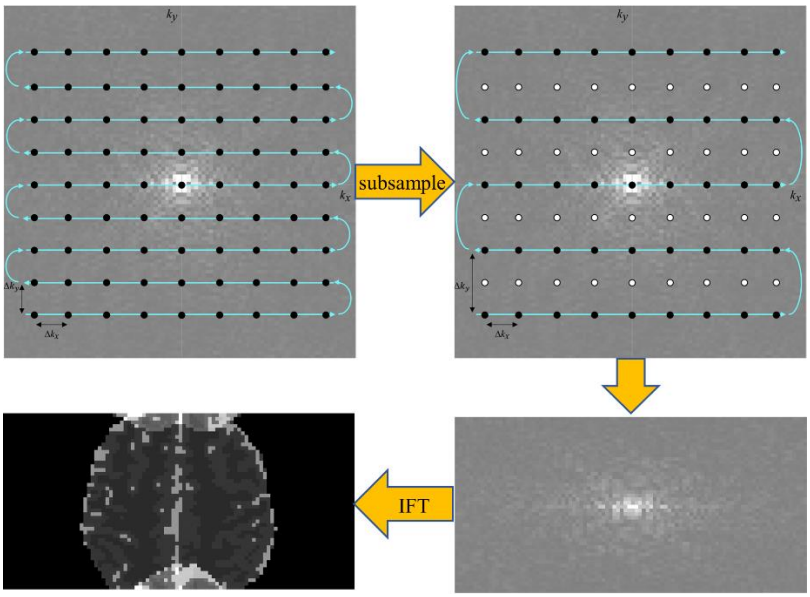


**Figure 1:** Full *k*-space array (top left), subsampled *k*-space array with $n_A = 2$ (top right), the acquired subsampled *k*-space array (bottom right), and aliased brain image (bottom left) after IFT of the subsampled *k*-space array.

To obtain a full field of view (FOV) image, the unacquired spatial frequencies need to be estimated to have full coil *k*-space arrays. The full *k*-space arrays for each coil are averaged to yield a single, full spatial frequency array. Then, the averaged, full *k*-space array is inverse Fourier transformed into a full brain image. A common method that estimates the unacquired coil spatial frequencies is GeneRalized Autocalibrating Partial Parallel Acquisition (GRAPPA) and was introduced by Griswold et al. (2002). GRAPPA operates in the spatial frequency domain before the IFT utilizing localized weights to interpolate the missing values in each coil *k*-space array. GRAPPA has its deficiencies, such as low image quality, a low signal-to-noise ratio (SNR), and diminished task detection power with higher acceleration factors. We propose a Bayesian approach to GRAPPA that will incorporate prior information, yielding increased SNR and image quality, with improved task detection power.

## 2. GRAPPA Technique

### 2.1 Reconstruction Process

As mentioned in Subsection 1.2, to measure less *k*-space data and still produce a full brain image, $n_C > 1$ receiver coils must be utilized. The process for GRAPPA is exhibited in Figure 2 with

an example of using $n_C = 4$ coils. The machine acquires subsampled spatial frequency arrays for each of the four coils shown in the top left of Figure 2. The top middle of Figure 2 displays the subsampled *k*-space arrays as fully arrays with the black dots indicating the acquired spatial frequencies and the white dots indicating the unacquired spatial frequencies. The unacquired spatial frequencies are estimated using GRAPPA image reconstruction, displayed as the green dots in the top right of Figure 2. This yields full coil *k*-space arrays as shown in the bottom right of Figure 2. To get a single full spatial frequency array (bottom middle), the full coil spatial frequency arrays are averaged together. The full spatial frequency is then reconstructed into a single, full field-of-view (FOV) brain image.

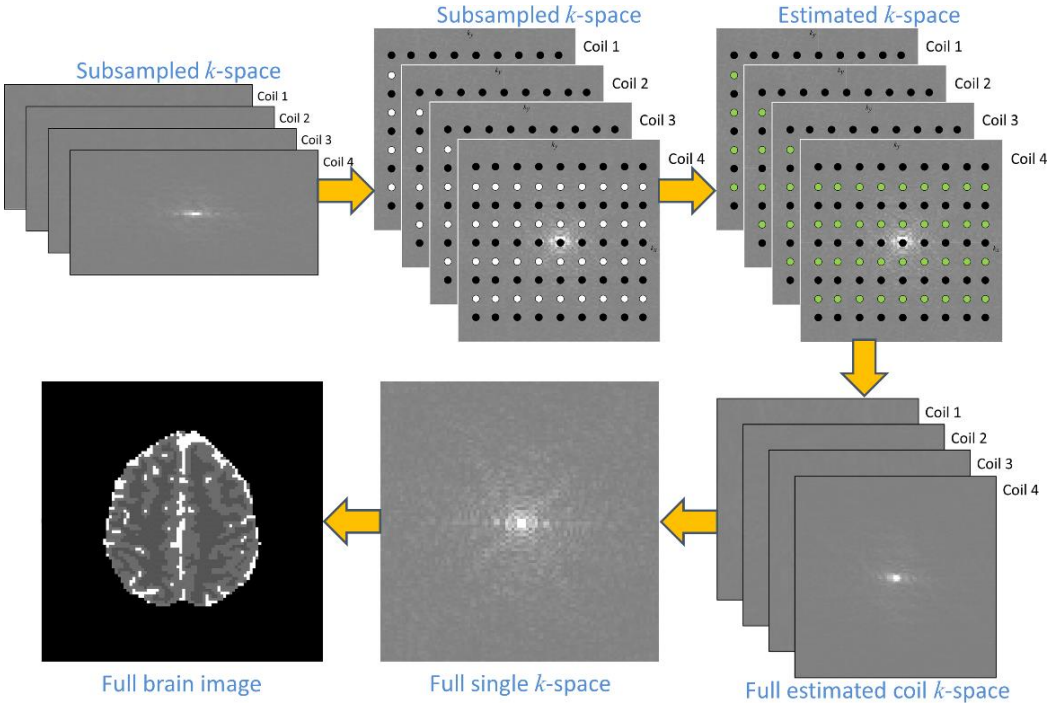


**Figure 2:** Subsampled *k*-space coil arrays (top left) that are spread to show a full k-space array where the black dots are the acquired spatial frequencies, and the white dots are the unacquired spatial frequencies (top middle). The missing spatial frequencies are then estimated (green dots in the top right) yielding full coil *k*-space arrays (bottom right). The full coil *k*-space arrays are then averaged together to produce a full spatial frequency array (bottom middle) which is then transformed into a full brain image (bottom left) using the IFT.

## 2.2 Model

In GRAPPA, the complex-valued localized weights are estimated using pre-scan coil calibration spatial frequency arrays. These coil calibration *k*-space arrays are fully sampled coil spatial frequencies arrays that are collected prior to the actual fMRI experiment. Kernels of varying sizes can be used to estimate the weights, creating a system of linear equations. Figure 3 illustrates how a 2×1 kernel is utilized to estimate the weights from the full coil calibration spatial frequencies with a four-channel coil array. In Figure 3, all the complex-valued data points are acquired, but are treated differently depending on the location of the data point. The black data points, $f_l$, are utilized as the "acquired" complex-valued spatial frequency values, the red points, $f_{calib}$, are the complex-valued calibration spatial frequency points, and the white points are ignored for the calculation of those weights. The white dots represent the spatial frequencies that would be unacquired during the fMRI experiment.

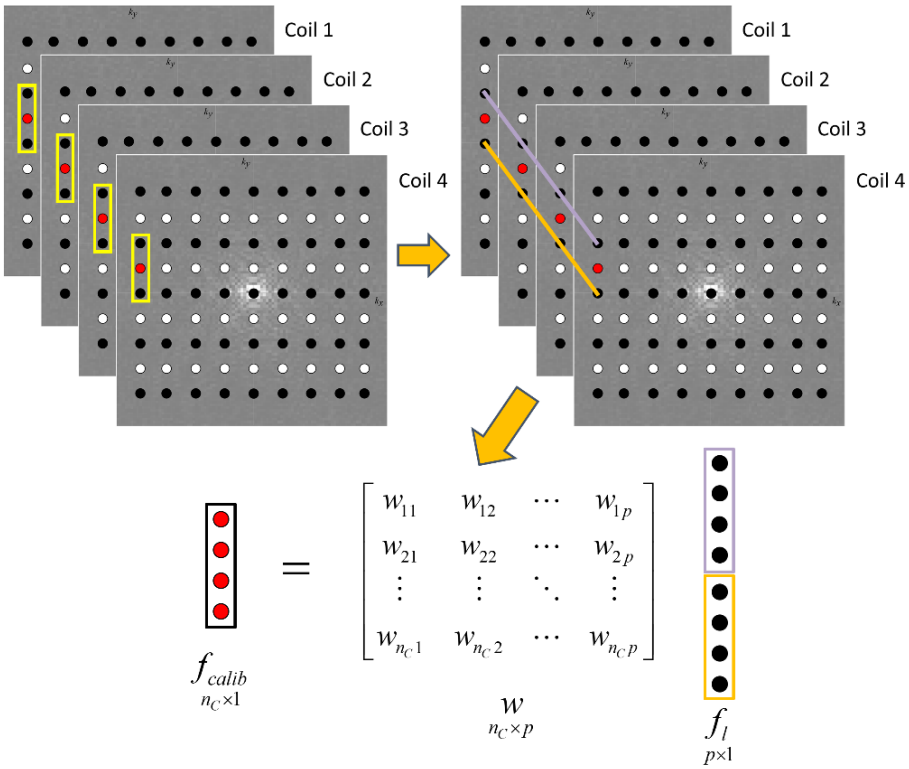


**Figure 3:** Subsampled *k*-space coil arrays (top left) that are spread to show a full *k*-space array where the black dots are the acquired spatial frequencies, and the white dots are the unacquired spatial frequencies (top middle). The missing spatial frequencies are then estimated (green dots in the top right) yielding full coil *k*-space arrays (bottom right). The full coil *k*-space arrays are then averaged together to produce a full spatial frequency array (bottom middle) which is then transformed into a full brain image (bottom left) using the IFT

The calibration points $f_{calib}$ and the "acquired" spatial frequencies $f_l$ along with the unacquired complex-valued weights, $w_c$, create a system of linear equations as displayed in Figure 3 (bottom). From the linear equations, we can estimate the weights $w_c$ using Eq. 2.1,

$$w_c^{(v)} = f_{calib}^{(v)} f_l^{(v)H} \left( f_l^{(v)} f_l^{(v)H} \right)^{-1}, \quad v = 1, \ldots, K \qquad [2.1]$$

where $w_c \in \mathbb{C}^{n_C \times p}$ is the complex-valued localized weights, $f_{calib} \in \mathbb{C}^{n_C \times 1}$ is the complex-valued calibration spatial frequencies, $f_l \in \mathbb{C}^{p \times 1}$ is the "acquire" spatial frequencies, $p = n_C k_{rows} k_{cols}$, $k_{rows}$ is the number of rows in the kernel, $k_{cols}$ is the number of columns in the kernel $H$ is the Hermitian or conjugate transpose, and $K$ is the total number of unacquired spatial frequencies in the subsampled *k*-space array. The process is repeated for each spatial frequency point that would be unacquired during the actual fMRI experiment (the white dots in Figure 3), yielding different localized weights for each of the unacquired spatial frequencies.

Once the weights for each of the unacquired coil spatial frequencies are estimated from the calibration *k*-space arrays, those weights are then utilized to interpolate the unacquired spatial frequencies in the actual fMRI experiment. The GRAPPA model with the estimated weights becomes

$$f_{ec}^{(v)} = w_c^{(v)} f_{kc}^{(v)} + \eta_c^{(v)}, \qquad v = 1, \ldots, K \qquad [2.2]$$

where $f_{ec} \in \mathbb{C}^{n_C \times 1}$ is the complex-valued interpolated spatial frequencies, $f_{kc} \in \mathbb{C}^{p \times 1}$ is the complex-valued acquired spatial frequencies, and $\eta_c \in \mathbb{C}^{n_C \times 1}$ is the additive complex-valued noise where

$\eta_c \sim N(0, \tau^2(1+i))$. The interpolated coil *k*-space values, $f_{ec}$, are inserted in the respective locations of each coil yielding full coil *k*-space arrays, as shown in Figure 2 (top right).

With GRAPPA image reconstruction, however, the resulting reconstructed brain images can have diminished SNR which is culminated from either a decreased signal intensity, increased temporal noise variance, or a combination of the two. With an increase in the temporal noise variance, this can lead to reduced power in task detection as well. These deficiencies motivate our Bayesian approach, which will allow for a more automated method for image reconstruction without having to potentially store and use large matrices. Unlike GRAPPA, our Bayesian approach will utilize all valuable available prior information and provide full distributions for the unacquired spatial frequencies, localized weights, and the residual *k*-space variance.

## 3. Bayesian Approach to GRAPPA

For our proposed Bayesian approach, we use a linear model like GRAPPA as expressed Eq. 2.2 except the acquired spatial frequencies will be the $f_{ec}$ variable instead of the $f_{kc}$ variable. Then the weights, $w_c$, and the unacquired spatial frequencies, $f_{kc}$, along with the residual *k*-space variance, $\tau^2$, are treated as unknowns with prior distributions placed on them. We also use an isomorphic real-valued representation of the linear GRAPPA model in Eq. 2.2 and is given by

$$\begin{bmatrix} f_{eR} \\ f_{eI} \end{bmatrix} = \begin{bmatrix} w_R & -w_I \\ w_I & w_R \end{bmatrix} \begin{bmatrix} f_{kR} \\ f_{kI} \end{bmatrix} + \begin{bmatrix} \eta_R \\ \eta_I \end{bmatrix}, \quad (\eta_R, \eta_I)' \sim N(0, \tau^2 I_{n_C}) \qquad [3.1]$$

where $f_{eR} \in \mathbb{R}^{n_C \times 1}$ and $f_{eI} \in \mathbb{R}^{n_C \times 1}$ are the real and imaginary components, respectively, of $f_{ec}$, $w_R \in \mathbb{R}^{n_C \times 1}$ and $w_I \in \mathbb{R}^{n_C \times 1}$ are the real and imaginary components of $w_c$, $f_{kR} \in \mathbb{R}^{p \times 1}$ and $f_{kI} \in \mathbb{R}^{p \times 1}$ are the real and imaginary components, respectively, of $f_{kc}$, $\eta_R \in \mathbb{R}^{n_C \times 1}$ and $\eta_I \in \mathbb{R}^{n_C \times 1}$ are the real and imaginary components, respectively, of $\eta_c$. This equation is a latent factor model with complex values and can be more compactly written as $f_e = wf_k + \eta$, where $f_e \in \mathbb{R}^{2n_C \times 1}$, $w \in \mathbb{R}^{2n_C \times 2p}$, $f_k \in \mathbb{R}^{2p \times 1}$, and $\eta \in \mathbb{R}^{2n_C \times 1}$ are the real-valued isomorphic representations of $f_{ec}$, $w_c$, $f_{kc}$, and $\eta_c$ respectively.

In this method, two different representations of the localized weights will be used. The first representation is the proper skew-symmetric design matrix $w \in \mathbb{R}^{2n_C \times 2p}$ as shown in Eq. 3.1. The second representation is $W = [w_R, w_I]$ which is used in the prior distribution and for parameter estimation of the localized weights. This is to ensure $w_R$ and $w_I$ are uniquely estimated for $w$ and do not need to be duplicated.

### 3.1 Data Likelihood, Prior, and Posterior Distributions

Like GRAPPA, we assume that the residual spatial frequency error is normally distributed in the real and imaginary components. So, the data likelihood for the acquired spatial frequencies for the $n_C$ coils is

$$P(f_e \mid w, f_k, \tau^2) \propto (\tau^2)^{-\frac{2n_C}{2}} \exp[-\tfrac{1}{2\tau^2}(f_e - wf_k)'(f_e - wf_k)]. \qquad [3.2]$$

We quantify available prior information about the unacquire spatial frequencies $f_k$, the localized weights $w$, and the residual *k*-space variance $\tau^2$ with assessed hyperparameters. The unacquired spatial frequencies $f_k$ are specified to have a normal prior distribution, as expressed in Eq. 3.3, since the real and imaginary components of fMRI data are assumed to be normally distributed (Lindquist, 2008). The localized weights $W$ are also specified to have a normal prior distribution (Eq. 3.4) and the *k*-space noise variance $\tau^2$ is specified to have an inverse gamma prior distribution (Eq. 3.5).

$$P(f_k \mid n_k, f_{k0}, \tau^2) \propto (\tau^2)^{-\frac{2p}{2}} \exp[-\tfrac{n_k}{2\tau^2}(f_k - f_{k0})'(f_k - f_{k0})], \qquad [3.3]$$

$$P(W \mid n_w, W_0, \tau^2) \propto (\tau^2)^{-\frac{2n_C p}{2}} \exp[-\tfrac{n_w}{2\tau^2} tr(W - W_0)(W - W_0)'], \qquad [3.4]$$

$$P(\tau^2 \mid \alpha_k, \delta) \propto (\tau^2)^{-(\alpha_k + 1)} \exp[-\tfrac{\delta}{\tau^2}], \qquad [3.5]$$

where *tr* is the trace of the $(W - W_0)'(W - W_0)$ matrix and the hyperparameters $n_k, f_{k0}, n_w, W_0, \alpha_k$, and $\delta$ are assessed from the pre-scan calibration spatial frequencies. The joint posterior distribution of the unacquire spatial frequencies $f_k$, the localized weights *w*, and the residual *k*-space variance $\tau^2$ is

$$P(w, f_k, \tau^2 \mid f_e) \propto P(f_e \mid w, f_k, \tau^2)\, P(f_k \mid n_k, f_{k0}, \tau^2)\, P(W \mid n_w, W_0, \tau^2)\, P(\tau^2 \mid \alpha_k, \delta) \qquad [3.6]$$

with the distributions specified from Equations 3.2, 3.3, 3.4, and 3.5.

### 3.2 Hyperparameter Assessment

The hyperparameters can be appropriately assessed in an automated way using the full pre-scan coil calibration spatial frequencies. For the BGRAPPA hyperparameter assessment, the same full calibration spatial frequencies and $f_{calib} = wf_l$ model are used like in GRAPPA reconstruction, but each spatial frequency point is treated differently than GRAPPA. As shown in Figure 4, the calibration spatial frequencies $f_{calib}$ for BGRAPPA are in the location of the data points where the acquired spatial frequencies are in the actual fMRI experiment. For GRAPPA, these data points are assigned to the $f_l$ variable in the $f_{calib} = wf_l$ model shown at the bottom of Figure 4. Using Eq. 2.1, this will result in the prior for the weights in BGRAPPA, $W_0$, to be different than the estimated weights utilized in GRAPPA image reconstruction. The $f_l$ points used for estimating the prior mean for the weights are assigned to be the prior mean of the unacquired spatial frequencies, $f_{k0}$.

The hyperparameters $n_k$ and $n_w$, which are the prior scalars of the prior means, are assessed to be the of calibration spatial frequencies $n_{cal}$. The average residual *k*-space variance over the coil spatial frequency arrays is calculated to obtain a prior mean for the residual *k*-space variance $\tau_0^2$. The hyperparameters $\alpha_k$ (shape parameter of the inverse gamma) and $\delta$ (scale parameter of the inverse gamma) are assessed to be $\alpha_k = n_{cal} - 1$ and $\delta = (n_{cal} - 1)\, \tau_0^2$. This prior information is incorporated to estimate the unacquired spatial frequencies in the subsampled *k*-space arrays.

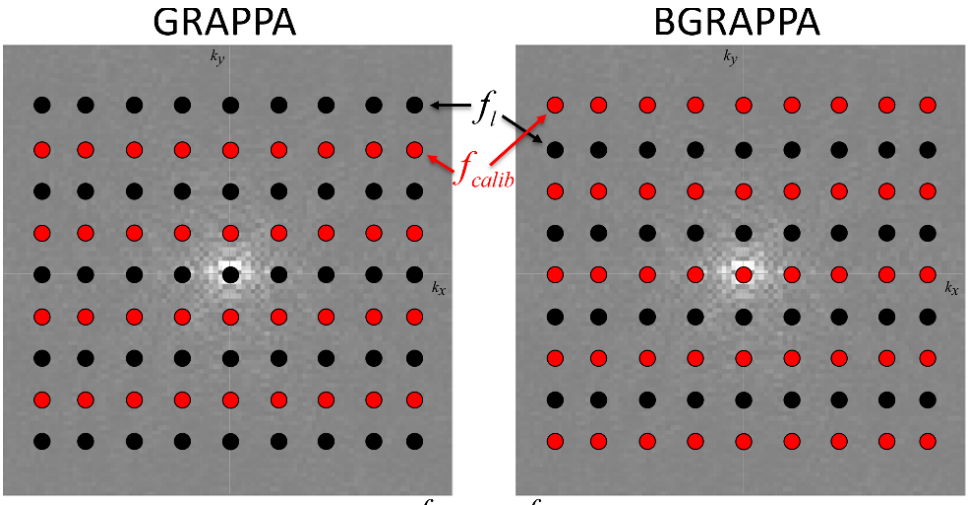


**Figure 4:** Full calibration *k*-space arrays that indicate which data points are used as $f_{calib}$ points and the $f_l$ points for GRAPPA (left) and BGRAPPA (right).

### 3.3 Posterior Estimation

Using the posterior distribution in Eq. 3.6, the Maximum *A Posteriori* (MAP) estimate for the unacquire spatial frequencies $f_k$, the localized weights *w*, and the residual *k*-space variance $\tau^2$ is estimated via the Iterated Conditional Modes (ICM) optimization algorithm (Lindley and Smith, 1972; O'Hagen, 1994). Beginning with the prior means for each parameter as initial estimates, the

ICM algorithm iterates over the parameters, calculating its posterior conditional mode until convergence at the joint posterior mode. The posterior conditional modes are

$$\hat{f}_k = \left(w'w + n_k I_{2p}\right)^{-1}(w'f_e + n_k f_{k0}), \quad [3.7]$$

$$\hat{w} = (F_e'F_k + n_w w_0)\left(F_k'F_k + n_w I_{2p}\right)^{-1}, \quad [3.8]$$

$$\hat{\tau}^2 = \frac{\Theta}{2(2n_C + 2p + 2n_C p + 1)}, \quad [3.9]$$

where $\Theta = \left(f_e - wf_k\right)'\left(f_e - wf_k\right) + n_k\left(f_k - f_{k0}\right)'\left(f_k - f_{k0}\right) + \alpha_k\delta + n_w tr[(W - W_0)(W - W_0)']$, $F_e = [f_{eR}, f_{eI}]$, and $F_k \in \mathbb{R}^{2p\times 2}$ is a skew symmetric matrix representation of the unacquired spatial frequencies $f_k$ as expressed by

$$F_k = \begin{bmatrix} f_{kR} & f_{kI} \\ -f_{kI} & f_{kR} \end{bmatrix}. \quad [3.10]$$

## 4. Simulation Study

### 4.1 Non-task Spatial Frequency Data

A noiseless non-task image was used to create two series of 510 simulated full coil images for one slice to mimic real-world MRI experimental data. A noiseless task image was also used along with the noiseless non-task image was used to create a series of 510 simulated full coil images for one slice mimicking real-world fMRI data. The simulated task activation was designed to mimic tapping of the subject's right fingers leading to activity in the left motor cortex which becomes our region of interest (ROI) for analyzing task detection in this experiment. Knowing this, artificial signal increase was added to the voxels in the ROI. With these three data sets, two separate experiments were run to test and compare BGRAPPA and GRAPPA.

For the first experiment, the last $n_{cal} = 30$ time points of the first non-task time series served as the calibration information utilized for hyperparameter assessment, and the second time series was used for simulating a subsampled non-task experiment. For the second experiment, the last $n_{cal} = 30$ time points of the second non-task time series served as the calibration information utilized for hyperparameter assessment, and the task series was used for simulating a real-world fMRI experiment. The complex-valued non-task and task images were multiplied by a designed sensitivity map with $n_C = 8$ coils. In real-world MRI experiments, the first few images of the time series have increased signal as the magnetization reaches a steady state. The first three images in the simulated series of images are appropriately scaled, based on the experimental data, replicating the increased signal. The series of images for both experiments were then Fourier transformed into full coil *k*-space arrays. The time series of coil *k*-space arrays were simulated by adding separate $N(0, 0.0036n_y n_x)$ noise, where $n_y$ and $n_x$ are the number of rows and columns, respectively, in the full *k*-space array, to the real and imaginary parts of full coil *k*-space arrays, corresponding to the noise in real-world fMRI experimental data. To mimic the fMRI experiment, the first 20 time points of the second time series in both experiments were discarded leaving 490 time points of spatial frequency arrays for the single slice. The remaining 490 time points in the time series were subsampled by censoring lines in *k*-space according to an acceleration factor of $n_A = 3$.

### 4.2 Reconstruction Results

To analyze the reconstruction performance of BGRAPPA vs. GRAPPA, we first reconstructed subsampled coil spatial frequencies at one time point, giving us a single unaliased image for both methods. For this, we used the first time point of the 490 simulated non-task time series with an acceleration factor of $n_A = 3$. Figure 5 shows the results of BGRAPPA (middle column) and GRAPPA (right column) for both magnitude (top row) and phase (bottom row) reconstructed images.

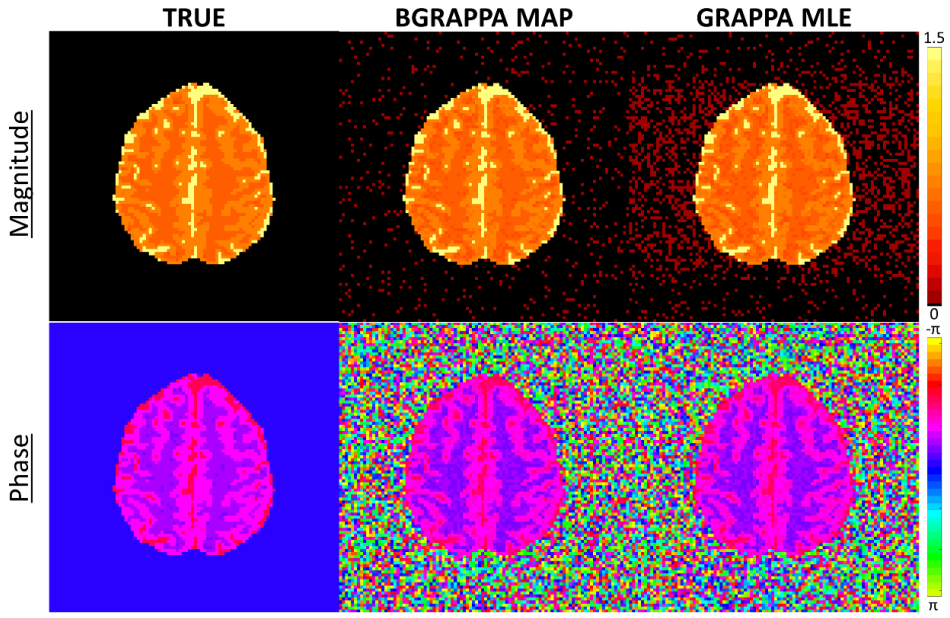


**Figure 5:** Magnitude (top row) and phase (bottom row) of the BGRAPPA (middle column) and GRAPPA (last column) reconstructed images compared to the true simulated images (left column).

Compared to the magnitude of the true simulated (left column), the BGRAPPA image reconstructed had decreased noise inside and outside the brain which indicates a more accurate reconstruction. Figure 6 shows Mean Squared Error (MSE) for the BGRAPPA and GRAPPA magnitude images compared to the true magnitude image. For both inside the brain ("In" in Figure 6) and outside the brain ("Out" in Figure 6), BGRAPPA has a noticeably smaller MSE compared to GRAPPA, further supporting a more accurate reconstructed image. The phase images for both methods closely resemble the true phase image shown in the bottom left of Figure 5.

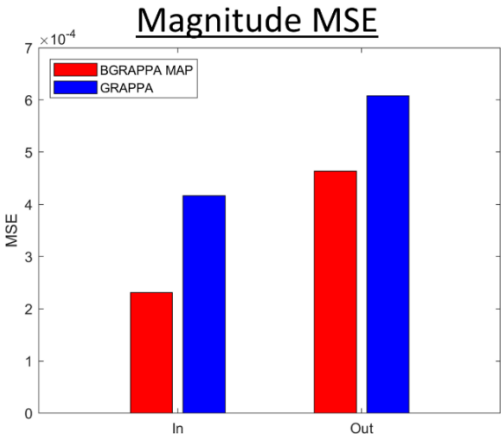


**Figure 6:** MSE for both inside and outside the brain for the BGRAPPA reconstructed magnitude image (red bars) and the GRAPPA reconstructed magnitude image (blue bars) when compared to the true simulated magnitude image.

Next, we analyzed the reconstruction of the entire non-task simulated time series from the first experiment with 490 time points and evaluated the temporal variance and the SNR for BGRAPPA and GRAPPA. In the left column of the Figure 7, we can see that the BGRAPPA (top row) had a

markedly lower temporal variance compared to GRAPPA (bottom row). This led to noticeably higher SNR (middle column of Figure 7) in the BGRAPPA reconstructed time series (top row) over the GRAPPA reconstructed time series (bottom row).

As mentioned in the introduction, the primary goal of fMRI is to analyze brain activity. The second simulated experiment was set up to test both BGRAPPA and GRAPPA in their power to detect task activation. The right column of Figure 7 displays the results of task detection for BGRAPPA and GRAPPA, with the ROI outlined in green, using 5% false discovery rate (FDR) threshold procedure (Benjamini and Hochberg, 1995). When evaluating the task detection results in Figure 7, we can see that BGRAPPA captures majority of the active voxels in our ROI where GRAPPA only captures one voxel indicating BGRAPPA having a stronger power of task detection.

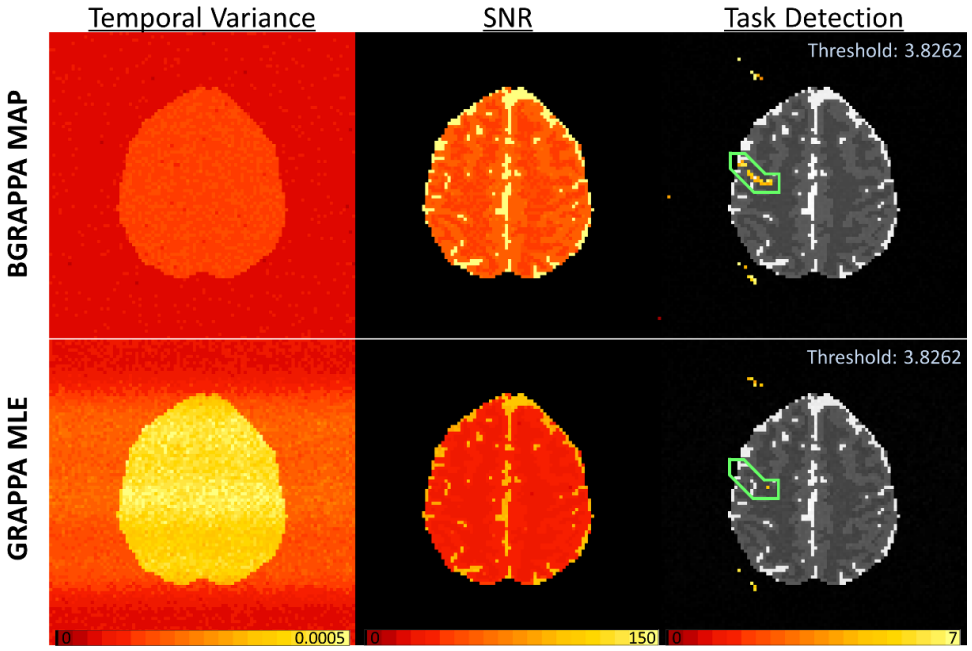


**Figure 7:** Temporal variance (left column), SNR (middle column) and task detection (right column) results for both BGRAPPA (top row) and GRAPPA (bottom row).

## 5. Discussion

### 5.1 Overview

In this research, we formulated a Bayesian approach to GRAPPA parallel fMRI image reconstruction. Our proposed BGRAPPA method treats the unacquired spatial frequencies, the localized weights, and the *k*-space noise variance as unknowns and places prior distributions on these parameters. Our Bayesian approach also incorporates more valuable prior information in estimating the unacquired spatial frequencies. The simulated results indicated a more accurate reconstructed image, a decreased temporal variance, and higher SNR with BGRAPPA. The task detection results also showed remarkably stronger power of task detection with BGRAPPA over GRAPPA.

### 5.2 Future Work

Future work with testing our BGRAPPA method would include utilization of different number of calibration spatial frequencies and applying different acceleration factors to the subsampled fMRI time series. More work with the simulated data will also include analysis of correlation between voxels and the voxels they were previously aliased with. After exhaustive testing using the simulated data sets, BGRAPPA will be applied to experimental fMRI data and compared to GRAPPA along the way.

## References


1. Bandettini P, Jesmanowicz A, Wong E, Hyde J. *Processing strategies for time-course data sets in functional MRI of the human brain.* Mag. Res. Med 30:161–173, 1993.
2. Benjamini, Y., Hochberg, Y. *Controlling the false discovery rate: a practical and powerful approach to multiple testing*. J. R. Stat. Soc. B, 57, 289 – 300, 1995.
3. Griswold MA, Jamob PM, Heidemann RM, Nikkka M, Jellus V, Wang J, Kiefer B, Haase A. *Generalized autocalibrating partially parallel acquisition (GRAPPA).* Mag. Res. Med, 47:1202–1210, 2002.
4. Hyde JS, Jesmanowicz A, Froncisz W, Kneeland JB, Grist TM, Campagna NF. *Parallel image acquisition from noninteracting local coils.* J. Mag. Res, 70:512–517, 1986.
5. Lindley DV, Smith AFM. *Bayes estimates for the linear model.* J. R Stat. Soc. B, 34 (1):1–18, 1972.
6. Lindquist, MA. *The statistical analysis of fMRI data.* Statistical Science 34, 1-18, 2008.
7. Ogawa S, Lee TM, Nayak AS, Glynn P. *Oxygenation-sensitive contrast in magnetic resonance image of rodent brain at high magnetic fields.* Mag. Res. Med 14(1):68–78, 1990.
8. O'Hagan, A. *Kendall's Advanced Theory of Statistics*. vol. 2B. Wiley, New York, 1994.
9. Pruessmann KP, Weiger M, Scheidegger MB, Boesiger P. *SENSE: Sensitivity Encoding for Fast MRI.* Mag. Res. Med, 42:952–962, 1999.
10. Rowe DB. *Image Reconstruction in Functional MRI. In Handbook of Statistical Methods for Brain Signals and Images*, Editors Ombao H, Lindquist M, Thompson W, Aston J. Chapman & Hall/CRC Press. p. 205-232, 2016.
11. Rowe DB. *Modeling both the magnitude and phase of complex-valued fMRI data*. Neuroimage, 25(4):1310–1324, 2005.
12. Rowe DB, Logan BR. *A complex way to compute fMRI activation*. Neuroimage, 23:1078–1092, 2004.